Identification of an Ideal Reactor Model in a Secondary Combustion Chamber

Charles A. Bass, Jr.
UTD Inc., Springfield, VA 22150

Robert B. Barat
New Jersey Institute of Technology, Dept. of Chemical Engineering, University Heights, Newark, NJ 07102

Paul M. Lemieux
U.S. Environmental Protection Agency, Office of Research and Development, National Risk Management Research Laboratory, Air Pollution Prevention and Control Division, Research Triangle Park, NC 27711

Tracer analysis was applied to a secondary combustion chamber of a rotary kiln incinerator simulator to develop a computationally inexpensive networked ideal reactor model and allow for the later incorporation of detailed reaction mechanisms. Tracer data from sulfur dioxide tracer experiments were reconstructed using a least-squares approximation that eliminated the intrinsic response of the measurement device and produced a residence time distribution between various points of the combustor. A model was chosen based on the best fit to tracer data, and consistency with physical geometry and temperature measurements. The resulting model showed that the active path was 1 s shorter than the mean residence time calculated from the total volumetric flow. The analysis found that complete mixing between the kiln gas and burner stream occurs farther downstream than originally expected. Results underscore the importance of turbulent mixing in reactor design and suggest that different design criteria are needed to ensure complete combustion.

Introduction

A model for a complex process such as combustion can be analyzed under a variety of conditions much faster and at a lower cost than these conditions can be replicated in bench- and pilot-scale experiments. Despite the rapid increase in computational power, modeling combustion processes requires trade-offs between detailed chemical kinetic modeling, involving hundreds to thousands of elementary reactions and intermediate compounds, and the detailed modeling approaches to turbulent mixing. Modeling the formation of Products of Incomplete Combustion (PICs) through numerous potential reaction pathways requires detailed chemical kinetics and, thus, demands simplified approaches to turbulent mixing. A networked ideal reactor model preserves the mathematical simplicity of an ideal reactor, while attempting to introduce some of the complexities of the mixing process. Ideal reactors provide a relatively simple mixing model to solve the large equation set generated by a detailed thermokinetic mechanism.

Practical systems such as a swirl burner in a furnace suggest a well-stirred zone followed by a plug-flow section. Beér and Lee (1965) investigated the mixing in this system by building a 1/10th scale water model and using a salt solution as a tracer to measure the residence time distribution (RTD), which agreed with the two-stage, perfectly stirred reactor (PSR) to the plug-flow reactor (PFR) model. Using a simple kinetic model for pulverized coal combustion, Beér and Lee demonstrated agreement between model and combustor as the flame swirl region was adjusted to alter the division between the PSR and PFR zones. Other approaches to ideal reactor model development have employed a combination of reactor geometry analysis and studies of temperature pro-

Correspondence concerning this article should be addressed to C. A. Bass, Jr.

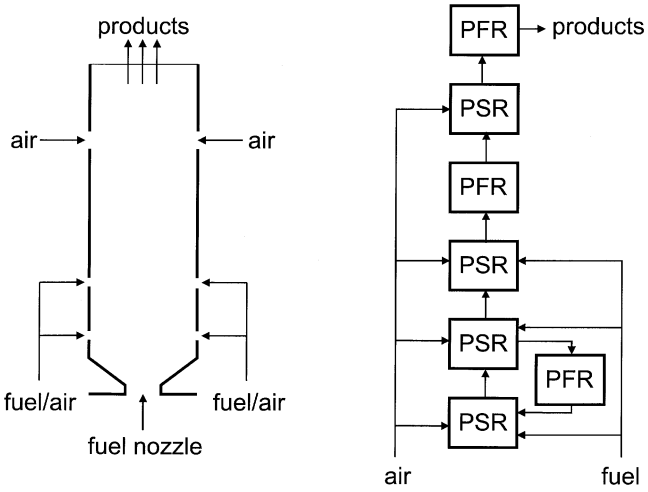

Figure 1. Ideal reactor model (right) developed for a turbine can combustor (left) (Swithenbank et al., 1972).

files, in combination with the application of empirical formulas that describe the turbulent discharge of a fluid from a nozzle (Beér and Chigier, 1983).

Swithenbank et al. (1972) relied primarily on reactor geometry when developing a 12-parameter ideal reactor model for a turbine combustor. A fuel-rich flame originated from a swirl nozzle and was successively augmented and diluted downstream from three sets of holes. The authors developed the model from the physical volumes between the fuel and air inlets to develop the ideal reactor network that was subsequently refined using the cross-section temperature profiles and cold-flow analysis (Figure 1). They successfully used the model to predict the rich blowoff limits of the combustor. Ewan et al. (1984) extended this study by measuring the RTDs between various points in the can combustor in a cold-flow mode which favorably compared with RTDs generated from computational fluid dynamic (CFD) models.

Mixing studies have been applied to full-scale mass burn incinerators using CFD models. In two separate studies, Ravichandran and Gouldin (1993) and Nasserzadeh et al. (1994) used transient two-dimensional (2-D) numerical simulations of tracer injection to determine mixing dynamics. Both studies emphasized the significance of reactor geometry, and the proper placement of burner jets to achieve a desired level of macromixing. They also highlighted the need for *in situ* tracer experiments that determine the RTD rather than relying on physical geometry to approximate the mean residence time.

This study applies tracer analysis to a secondary combustion chamber (SCC) of a rotary kiln incinerator simulator (RKIS) pilot-scale system to develop a computationally inexpensive mixing model that makes reasonable approximations of the actual flow characteristics in order to allow for the incorporation of detailed reaction mechanisms. The objective of this work is not to resolve the true mixing characteristics of the reactor, but to find a networked ideal reactor model that is consistent with observation and approximates the mixing characteristics for the application of the detailed reaction mechanism.

Approach

The strategy of constructing an ideal reactor model involves first considering the observed characteristics of that system such as temperature, geometry, and RTD, then identifying the model parameters. The SCC will be modeled based on the assumption that the passage of a stable gaseous tracer through the reactor can be described with a set of linear first-order differential equations, a condition that applies to a reactor that can be described by a network of ideal reactors, and, when normalized, does not depend on the initial concentration of the tracer. Unless the tracer is consumed or adsorbed, this assumption normally holds true.

Modeled system

A linear system that has a single input and a single output (SISO), such as the tracer injected at a single point and measured by an analyzer at a single point downstream as a function of time t can be described by a single transfer function $g(t)$. The output of the system $y(t)$ is a convolution of the input $u(t)$ with the transfer function

$$y(t) = \int_0^t g(t-\tau)u(t)d\tau \qquad (1)$$

where τ is the dummy time variable. For the tracer experiments, the system represents the effects of both the reactor and the analyzer on the measure response of the tracer (Figure 2a). As a linear SISO system, the sequence of the reactor and analyzer does not matter. This provides an alternate view where the output of the analyzer can be considered as the input of the reactor (Figure 2b). Using this view, the analyzer step response is the input $U(t)$ and the analyzer impulse response will be represented as $u(t)$. Only the analyzer step

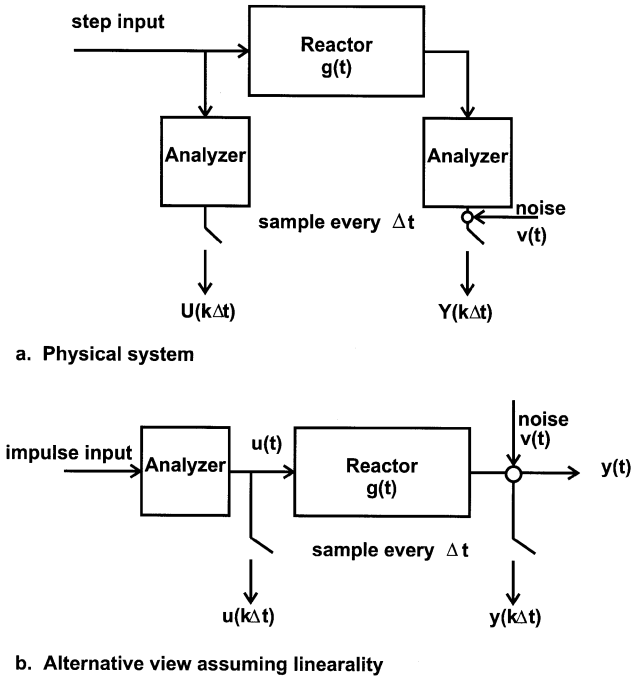

Figure 2. Modeled system.

response is directly measured. However, differentiating the analyzer step response with respect to time gives the analyzer impulse response, which will be referred to simply as the analyzer response (Levenspiel, 1972)

$$u(t) = \frac{dU(t)}{dt} \tag{2}$$

In the same fashion, differentiating the system step response $Y(t)$ gives the system response $y(t)$. The system response is the combined response of the tracer through the analyzer and the reactor with the addition of any uncorrelated noise external to the analyzer or reactor $v(t)$. For a continuous system

$$y(t) = \int_0^t g(t-\tau)u(t)d\tau + v(t) \tag{3}$$

Least-squares estimation of the RTD

The RTD is the distribution of times spent by each infinitesimal packet of fluid measured at the reactor exit. When the reactor is a SISO linear system, the transfer function $g(t)$ in the modeled system (Figure 2) is also the RTD $E(t)$ (Himmelblau and Bischoff, 1968). This can be identified from the input $U(t)$ and output $Y(t)$. Hsia (1977) provides a suitable technique which identifies this function as the estimator of a least-squares formula. This method computes the autocorrelation (input) and cross-correlation (input vs. output) functions in the process, so the input signal must be stationary. That is, the expected value is invariant with time (Hsia, 1977). The step input function does not meet this criterion. However, converting the step input and response function to an impulse input and response by using the first derivative (Levenspiel, 1972) makes it a quasi-stationary process. A Savitsky-Golay (Press et al., 1992) filter that fits a second-order polynomial to a window 10 points on each side of a given point estimates the derivative by using the polynomial coefficients estimated at each point.

The system has a continuous input and output, but it is sampled on a discrete time interval Δt. When Δt is small, relative to the system response, a discrete system approximation becomes a valid approach. Equation 3 can be approximated as a discrete system by defining the weighting function h

$$h(k\Delta t) = \Delta t g(k\Delta t) \tag{4}$$

where k is the sample index (where $t = k\Delta t$ for $k = 1, 2, 3 \ldots$). Equation 5 gives the discrete version of Eq. 3

$$y(k\Delta t) = \sum_{i=k-p}^{k} h(k\Delta t - i\Delta t)u(i\Delta t) + v(k\Delta t) \tag{5}$$

Here, p is an integer such that $g(t) \approx 0$ for $t \geq p\Delta t$ and $0 \leq k \leq p$. The discrete system response $y(k\Delta t)$ depends on the weighted discrete analyzer response $u(i\Delta t)$ for the preceding p measurements or $i = k-p, k-p+1, \ldots, k$.

Despite the fact that the experiment measured a single system response to a single input, it is necessary, for this method, to consider the experiment as a periodic series of responses to a periodic series of inputs where the system has time to come to rest after each input. The system response is measured for an interval between 0 and p where p is chosen large enough for $y(t) \approx 0$ for $t \geq p\Delta t$. Equation 5 can now be expressed in matrix form

$$\boldsymbol{y} = \boldsymbol{U}\boldsymbol{h} + \boldsymbol{v} \tag{6}$$

where

$$\begin{aligned}
\boldsymbol{y} &= \begin{bmatrix} y(0) & y(1) & \cdots & y(p) \end{bmatrix}^T \\
\boldsymbol{v} &= \begin{bmatrix} v(0) & v(1) & \cdots & v(p) \end{bmatrix}^T \\
\boldsymbol{h} &= \begin{bmatrix} h(0) & h(1) & \cdots & h(p) \end{bmatrix}^T \\
\boldsymbol{U} &= \begin{bmatrix} u(0) & u(-1) & \cdots & u(-p) \\ u(1) & u(0) & \cdots & u(1-p) \\ \vdots & \vdots & \ddots & \vdots \\ u(p) & u(p-1) & \cdots & u(0) \end{bmatrix}
\end{aligned} \tag{7}$$

and the superscript T denotes the matrix transpose. Applying the matrix form of the linear least-squares formula (Draper and Smith, 1998) to Eq. 6 gives the estimator of $\boldsymbol{h}$. Equation 8 is the estimate of the $\boldsymbol{h}$ vector ($\hat{\boldsymbol{h}}$) that minimizes the sum of the squared errors $\boldsymbol{v}^T\boldsymbol{v}$

$$\hat{\boldsymbol{h}} = (\boldsymbol{U}^T\boldsymbol{U})^{-1}\boldsymbol{U}^T\boldsymbol{y} = \boldsymbol{\Phi}^{-1}\boldsymbol{\Gamma} \tag{8}$$

Here, $\boldsymbol{\Phi}$ and $\boldsymbol{\Gamma}$ represent the groupings that relate to the autocorrelation and cross-correlation vectors, respectively, shown in Eq. 9

$$\boldsymbol{\Phi} = \frac{1}{1+p}\boldsymbol{U}^T\boldsymbol{U} = \begin{bmatrix} \varphi_{uu}(0) & \varphi_{uu}(1) & \cdots & \varphi_{uu}(p) \\ \varphi_{uu}(1) & \varphi_{uu}(0) & \cdots & \varphi_{uu}(p-1) \\ \vdots & \vdots & \ddots & \vdots \\ \varphi_{uu}(p) & \varphi_{uu}(p-1) & \cdots & \varphi_{uu}(0) \end{bmatrix}$$

$$\boldsymbol{\Gamma} = \frac{1}{1+p}\boldsymbol{U}^T\boldsymbol{y} = \begin{bmatrix} \varphi_{uy}(0) \\ \varphi_{uy}(1) \\ \vdots \\ \varphi_{uy}(p) \end{bmatrix} \tag{9}$$

The autocorrelation function φ_{uu} of the inputs $\boldsymbol{u}$ and cross-correlation function φ_{uy} of the inputs $\boldsymbol{u}$ with the outputs $\boldsymbol{y}$ in the discrete form are defined by

$$\begin{aligned}
\varphi_{uu}(k) &= \frac{1}{1+p}\sum_{j=0}^{p} u(j)u(j-k) \\
\varphi_{uy}(k) &= \frac{1}{1+p}\sum_{j=0}^{p} u(j-k)y(j)
\end{aligned} \tag{10}$$

Using this least-squares approach eliminates the uncorrelated noise $v(k\Delta t)$ from the solution. A problem arises, however, when finding the inverse of $\boldsymbol{\Phi}$, which is rank deficient

and, thus, singular or near singular. Hence, $\mathbf{\Phi}^{-1}$ cannot be determined by standard techniques such as Gaussian elimination. This also means that $\hat{\boldsymbol{h}}$ will not have a unique solution (Draper and Smith, 1998). Rather than dwell on the implications here, it is sufficient to select an approach to solve for $\hat{\boldsymbol{h}}$ without directly computing $\mathbf{\Phi}^{-1}$ and apply that approach consistently. A constrained iterative reconstruction technique (Schafer et al., 1981) was chosen to find $\hat{\boldsymbol{h}}$.

Analysis of moments

The moments of the reconstructed RTDs were analyzed as part of the process of gaining insight into the number and location of the mixing regions. The first three moments of the RTD—the mean (μ), variance (σ^2), and skewness coefficient (s^3)—are shown below in their discrete form (Levenspiel, 1972; Fogler, 1992)

$$\mu = \frac{\sum_{i=0}^{p} E_i t_i}{\sum_{i=0}^{p} E_i}, \quad \sigma^2 = \frac{\sum_{i=0}^{p} E_i t_i^2}{\sum_{i=0}^{p} E_i} - \mu^2,$$

$$s^3 = \frac{1}{\sigma^3}\left(\frac{\sum_{i=0}^{p} E_i t_i^3}{\sum_{i=0}^{p} E_i} - 3\mu\sigma^2 - \mu^3 \right) \tag{11}$$

Before discussing the moments calculated from the experimental results, it is useful to consider them in the context of ideal reactor models. Consider three archetype ideal reactor models: (1) PSR and PFR in series with mean resident times τ_1 and τ_d, respectively; (2) two different size PSRs in series with mean residence times τ_1 and τ_2; and (3) n equal PSRs in series, each with mean residence time τ_i. Table 1 shows the RTD formulas and resulting moments, derived from the continuous versions of Eq. 11.

From these archetypes, several deductions may be made. First, for a simple series with no recirculation, the PFR makes no contribution to the variance and skewness coefficient, and PSR mean residence time for archetype 1 is better measured through the variance. Next, the skewness coefficient has a value of 2 for a single PSR in that series and becomes smaller as more PSRs are added. Finally, for the series of equal-sized PSRs (archetype 3), the number of reactors in the series can be deduced from the skewness coefficient; however, higher moments heavily weight perturbations farthest from the mean, and, thus, are less reliable. A better deduction can be made from the first two moments (Fogler, 1992)

$$n = \frac{(n\tau_i)^2}{n\tau_i^2} = \frac{\mu^2}{\sigma^2} \tag{12}$$

Parameter identification

The model parameters were determined by directly fitting the model to the normalized tracer step response rather than to the reconstructed RTDs. This method has the advantage of fitting the model to original data. The process uses an iterative approach to minimize the error defined by the least-squares criterion. The Nelder-Mead simplex search routine (Nelder and Mead, 1965) performs the parameter adjustment to minimize the squares of the errors. The model uses the analyzer step response $U(k\Delta t)$ as input along with an initial "guess" of the parameters and gives the model step response or estimated step response $\hat{Y}(k\Delta t)$, by

$$\hat{Y}(k\Delta t) = \sum_{i=k-p}^{k} \hat{g}(k\Delta t - i\Delta t; \boldsymbol{\alpha}) U(i\Delta t) \tag{13}$$

where $\boldsymbol{\alpha}$ is the parameter vector and $\hat{g}$ is the model that estimates the transfer function of the system.

The modeled transfer function $\hat{g}$ of an ideal reactor network is more conveniently handled as a Laplace transform, because the basic building blocks, the PSR and PRF, are easily represented in algebraic combination. The linear simulation (LSIM) function in the MATLAB control toolbox can use the analyzer step response $U(k\Delta t)$ to drive the resulting numerator and denominator polynomials of the transfer function to produce a simulated output. Equation 14 shows the Laplace transform for the PSR

$$G(s) = \frac{a_r}{s + a_r} \tag{14}$$

Here, a_r is $1/\tau_r$, the reciprocal of mean residence time, $\boldsymbol{G}(\boldsymbol{s})$ is the transfer function or the RTD of the PSR, and $\boldsymbol{s}$ is the independent variable in the Laplace domain. For a PFR, the equation is an exponential function

$$G(s) = e^{-\tau_d s} \tag{15}$$

Although the exponential form does not algebraically complicate the network transfer function in the Laplace domain, it does not give a convenient polynomial as required by LSIM.

Table 1. Moments of Model Archetypes.

	RTD	Mean (μ)	Variance (σ^2)	Skewness (s^3)
(1) PSR to PFR	$E(t) = \frac{e^{(\tau_d - t)/\tau_1}}{\tau_1} \tau \geq \tau_1$	$\tau_d + \tau_1$	τ_1^2	2
(2) Two PSRs $\tau_1 \neq \tau_2$	$E(t) = \frac{e^{-t/\tau_1} - e^{-t/\tau_2}}{(\tau_1 - \tau_2)}$	$\tau_1 + \tau_2$	$\tau_1^2 + \tau_2^2$	$\frac{2(\tau_1^3 + \tau_2^3)}{(\tau_1^2 + \tau_2^2)^{3/2}}$
(3) Multiple PSRs	$E(t) = \frac{t^{(n-1)}}{(n-1)!\tau_i^n} e^{-t/\tau_i}$	$n\tau_i$	$n\tau_i^2$	$\frac{2}{\sqrt{n}}$

Rather than trying to approximate the exponential as a polynomial, the PFR was introduced as a time domain delay of τ_d after the LSIM calculation.

Experimental Work

Figure 3 shows the RKIS and SCC located at the U.S. EPA's National Risk Management Research Laboratory, Air Pollution Prevention and Control Division, in Research Triangle Park, NC. The system includes the salient features of a commercial rotary kiln system. The 73-kW (250,000-Btu/h) SCC is attached to a 73-kW pilot-scale rotary kiln incinerator. Both burners use natural gas as the primary fuel. The SCC contains a removable choke which divides the mixing section from the burnout section. During SCC experiments, liquid surrogate wastes were injected at point B2 in the kiln transition duct using a nitrogen (N_2)-and-air atomizer (Lemieux et al., 1996).

The geometry of the SCC gives a starting point for model synthesis by identifying distinct mixing regions that might be modeled as ideal reactors. The two section design of the SCC automatically suggests at least two mixing zones divided by the choke: the mixing section and the burnout section. The tangential entrance of the gases from the kiln transition duct into the mixing section forces a cyclone chamber-like swirl, while the SCC burner creates another co-rotating swirl through adjustable vanes of the fuel and air inputs. However, since the mixing chamber has two sources of swirl from two separate feeds, the result may be two mixing zones and possibly a third representing an entrainment zone between them. Additionally, there is potential for another mixing zone downstream of the choke as the emerging gases slow to the bulk velocity in the burnout section. Hence, the geometry of SCC suggests the existence of up to four mixing zones that might be modeled as PSRs.

Tracer studies

Tracer studies, using sulfur dioxide (SO_2) as the tracer gas, identified the RTD of the mixing and the burnout sections of the SCC. The main kiln burner and SCC afterburner were

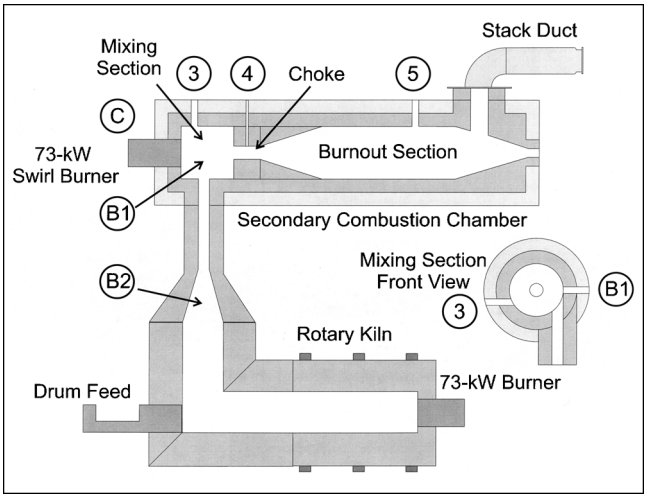

Figure 3. Rotary kiln incinerator simulator (RKIS) and the secondary combustion chamber (SCC).

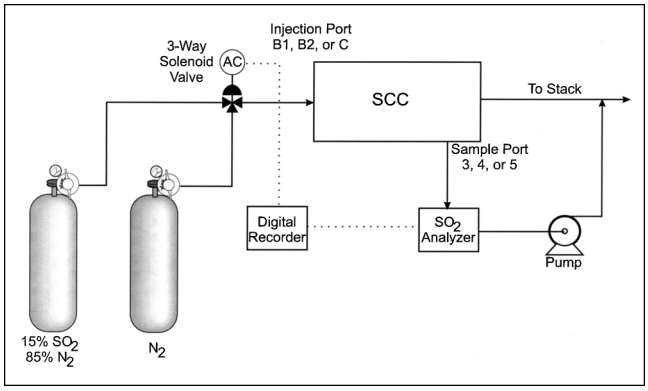

Figure 4. SO_2 tracer experiment setup.

operated at constant fuel/air conditions. These correspond to an overall fuel/air equivalence ratio (the fuel/air equilivalence ratio, φ, is the mass ratio of fuel to air divided by the stoichiometric mass ratio of fuel to air, where $\varphi < 1$ is fuel lean) of 0.92 with 2.42×10^4 std cm^3/s (30.0 g/s) entering through the kiln transition duct and 1.28×10^4 std cm^3/s (15.8 g/s) entering through the SCC swirl burner. Figure 4 shows the experimental setup. Tracer gas entered the system as step input. Experimental runs were conducted with the tracer injected at either the side of the mixing chamber (B1), the kiln/SCC transition duct (B2), or through the swirl burner (C). At different experimental runs, the tracer was sampled either at side of the mixing chamber (3) opposite to B1, the choke (4), or near the end of the burnout section (5) (see Figure 3). The analyzer was limited to a minimum digital sampling interval of 0.05 s and had its own characteristic response. This was separately measured using the same sample train. A typical run had three sample sequences with each sequence consisting of a stepup and stepdown response. However, due to sampling train difficulties, the integrity of the system response stepup data was suspect and thus rejected.

Temperature profiles

Temperature profiles were taken along the horizontal and vertical diameter midway in the mixing chamber, on the vertical diameter midway in the burnout section, and midway on the vertical diameter in the choke. The experimenters used a suction pyrometer for the mixing chamber and burnout section temperatures and a type R thermocouple in the choke. The temperature was recorded at 2.54 cm (1 in.) intervals. A temperature correction for radiation heat from the R-type thermocouple was done using a Nusselt number correlation to estimate the heat transfer across the boundary layer (Fristrom, 1995, p. 119) the measurements from the shield suction pyrometer did not require this adjustment.

Figure 5 shows a rendered contour temperature profile in the mixing chamber. The rendering shows the presence of a relatively tight flame region and suggests the presence of at least two distinct mixing zones in the chamber. The alignment of the kiln transition duct is depicted on the graph. This graph displays the effect of the cooler gas entering the chamber on the right and the relatively small flame zone of the swirl burner near the axial centerline. Using the 1,050 K

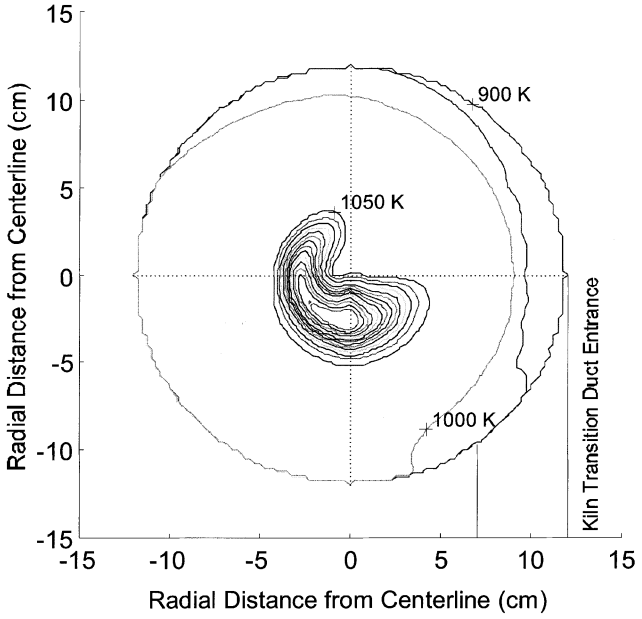

Figure 5. Radial temperature profile—SCC mixing section.

Temperature contours from 900 to 1,700 K at 50-K increments.

contour as an approximation of the flame zone boundary, the flame cross section occupies 10.2% of the reactor cross-section area and has an average (weighted on the heat capacity of N_2) temperature of 1,343 K. Using the same weighting technique, the reactor cross-section has an average temperature of 1,009 K.

Figure 6 shows the vertical temperature profiles in the choke and the burnout section. Since the choke measurement did not use a suction pyrometer, the temperatures shown on the graph have been corrected for radiation heat for a spherical thermocouple bead (Fristrom, 1995, p. 119).

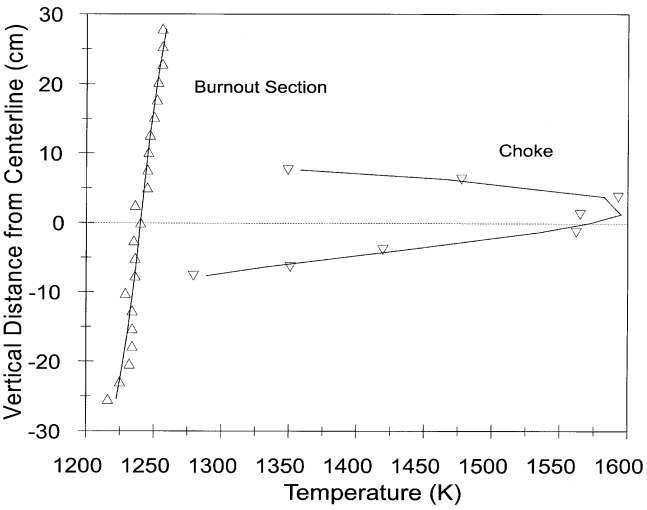

Figure 6. Vertical temperature profile in the choke and burnout section.

This graph indicates a significant temperature difference (300 K) between the gas near the lower choke wall and the gas just above the center in the choke, which reveals the presence of two distinct, but converging, temperature zones. Since the choke wall heavily insulates the passage, heat loss through the walls would not account for this behavior. Downstream, in the burnout section, the temperature profile is approximately even with a slight degree of buoyant stratification. This suggests that streams converge past the choke and should be modeled as a single homogenous (mixed) stream. Using the same analysis conducted for the mixing section, the average cross-section temperatures for the choke and the burnout section (at point 5) were found to be 1,213 and 967 K, respectively.

Results and Analysis

Each tracer run had at least three data sets of the step-down system and analyzer responses. To use these data in the least-squares reconstruction of the RTD, the information from each of these samples was normalized, combined, differentiated using a Savitsky-Golay filter (Press et al. 1992), and resampled at a constant interval t for the input function $u(k\Delta t)$ and the response function $y(k\Delta t)$. Figure 7 shows the normalized responses and transfer function derived from data gathered from a tracer runs using the port B1 input and sampled at port 4 (Figure 3). $E(k\Delta t)$ is the least-squares reconstruction estimate of the transfer function $\hat{g}(k\Delta t)$ equal to $\hat{h}(k\Delta t)/$t. The estimate of the system response function $\hat{y}(k\Delta t)$ is given by

$$\hat{\boldsymbol{y}} = \boldsymbol{U}\hat{\boldsymbol{h}} \tag{16}$$

An RTD was derived for each run using the least-squares reconstruction estimate. The first three statistical moments from each RTD were used to gain more insight on the macromixing processes taking place.

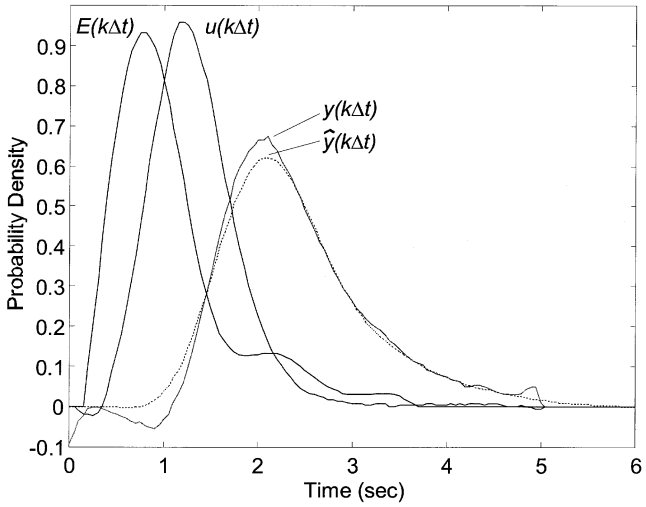

Figure 7. Reconstructed RTD $E(k\Delta t)$, from the system response, $y(k\Delta t)$, and the analyzer response $u(k\Delta t)$.

Estimated system response $y(k\Delta t)$ shown for comparison.

Table 2. Moments from Tracer Runs

Run*	In/Out Port	Mean (s)	Variance (s^2)	Skewness Coeff.
Average	Analyzer	1.30	0.21	1.67
T1	B1/3	0.56	0.32	2.57
T2	B1/4	1.08	0.40	1.45
T3	B1/5	3.59	2.13	0.68
T4	B2/3	0.86	0.26	1.36
T5	B2/4	1.38	0.60	1.12
T7	B2/5	3.99	2.00	0.68
T8	C/4	0.31	0.17	2.03
T10	C/5	3.60	1.71	0.76

*Runs T6 and T9 were pulse rather than step inputs and lacked a sufficiently strong response for analysis.

Table 2 lists the results of these moment calculations for the tracer runs. These show consistency with the physical configuration shown in Figure 3. The mean residence time and the variance increased as the tracer was collected from sampling ports farther downstream. The mean residence time derived from the RTD differs from spatial time $V\bar{\rho}/\dot{m}$ (reactor volume times mean density over mass-flow rate), due to the presence of dead space.

Referring back to the model archetypes in Table 1, the variance listed in Table 2 reveals the nature of mixing: for pure plug-flow sections, $\sigma_i^2 = 0$; for PSR sections, $\sigma_i^2 = \tau_i^2$; and for an ideal reactor series, the variance is additive from one section of the reactor to the other, as demonstrated with archetype 2. From this fact, variance should increase when sampled further downstream, which was generally observed. However, higher moments weight measurements are furthest from the mean, which are most susceptible to noise and least accurate.

Despite its questionable accuracy, the skewness coefficient reveals a trend. In the multiple PSR archetype, the skewness coefficient decreases with the number of reactors. As the sample point moved downstream away from the injection point, the skewness coefficient decreased, indicating additional (PSR) mixing zones. The RTD of a PSR gives a skewness coefficient of 2 in contrast to a PFR (with or without Gaussian diffusion), which has a skewness coefficient of zero. For ideal reactor models, the RTD of PSRs in series approaches that of a PFR as more reactors are added (Levenspiel, 1972). The RTDs from B1 to 3 and C to 4 have a skewness near 2, indicating a distinct single mixing region for each of these streams. Using the skewness coefficient formula derived for multiple reactors and solving for n gives

$$n = \left(\frac{2}{s^3}\right) \tag{17}$$

Using this formula, $n = 0.61$ for B1 to 3, and $n = 0.97$ for C to 4. This is further reinforced by applying Eq. 12 for multiple PSRs in series, which gives $n = 0.98$ for B1 to 3 and $n = 0.57$ for C to 4. Since relying on higher moments is subject to error, no single tool is absolute. However, the combination of both of these approaches reinforces a conclusion of a single mixing area between B1 and 3 and another between C and 4. This also suggests that very little, if any, of the afterburner gas (C to 4) contributes to a postulated entrainment.

The B1 to 4 RTD has a smaller skewness coefficient that could indicate the presence of an additional mixing region for the kiln gas stream prior to the choke. Applying Eq. 12 gives $n = 2.9$, and applying Eq. 17 gives $n = 1.9$. This reinforces the assertion of an additional mixing zone after point 3 and prior to the choke. The skewness coefficients for the C to 5 and B1 to 5 RTDs are much smaller, which supports a model of two or three additional PSRs between the choke and point 5. Using the moments of the reconstructed RTDs along with inferences from the temperature profiles and geometric factors, models can be synthesized for parameter identification.

Model synthesis

Figure 8 shows the base line model (model 0) that was developed based on the SCC geometric configuration, and physical observations including temperature profiles, reconstructed RTDs, and the analysis of moments. Model 0 was the simplest approach, consistent with observations, and has four distinct mixing or recirculation zones. Zone 1 is the recirculating flame from the SCC swirl burner. This phenomenon is well documented by Beér and Chigier (1983) and modeled, as a well stirred reactor by Beér and Lee (1965). The radial cross-section temperature profile (Figure 5) and RTD moments (Table 2) further validate treating the flame zone as a distinct region. Zone 2 comes from the swirling flow created by the tangential entry of the kiln gas into the mixing section, which is again reinforced by the cross-section temperature profile and the RTD moments. The geometry of the mixing chamber affects the confluence of these two regions. Forcing both flows through a narrow choke should create an entrainment region in the mixing section. Zone 3 is likely formed by the swirling gases that emerge from the choke. The mixing section resembles a tangential-entry swirl burner (Syred and Beér, 1974; Beér and Chigier, 1983; Hallett, 1986) feeding the burnout section. The tangential entry of the kiln gas creates a large axial flux of angular momentum that transfers through the choke to create Zone 4 in the same manner as the nozzle on a swirl burner. The dimensionless angular momentum flux or swirl number S quantifies the intensity of this swirl (Beér and Chigier, 1972). The divergent exit into the burnout section enlarges the recirculating zone (Syred and Beér, 1974). After Zone 4, the flow should approximate a PFR.

In Figure 8, each box represents an ideal reactor. Each of the five reactors has two parameters: the mean residence time τ and the reactor temperature T (or entrance temperature

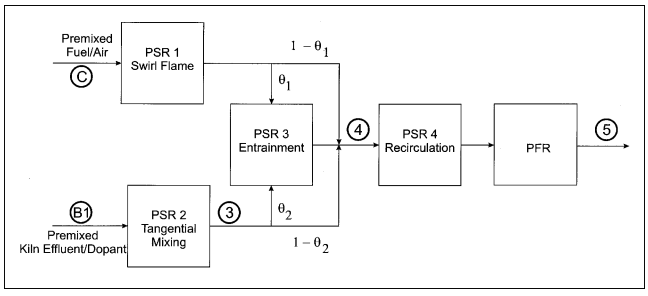

Figure 8. Postulated ideal reactor model (model 0).

for the PFR). The addition of the two mixing fraction parameters θ_1 and θ_2, which depict the fractions of the burner gas stream and kiln effluent stream mixing prior to the choke, makes the figure a 12-parameter model. This is the simplest possible model when geometry and observed temperature profiles are considered. Since the SCC may contain dead space, the total volume cannot be used to eliminate a degree of freedom. The dead volume is not included on the schematic because its parameter is found through physical closure and does not add to the parameter count. The next step is to identify the parameters.

The model depicted in Figure 8, translated into formulas for each specific input-to-output combination corresponding to a data set for the mixing section and expressed in Laplace domain, is given in Eqs. 18a–18c

$$\text{B1 to 4:}\quad G(s)=\frac{\theta_2 a_2 a\varepsilon}{(s+a_2)(s+a_3)}+\frac{(1-\theta_2)a_2}{(s+a_2)} \tag{18a}$$

$$\text{C to 4:}\quad G(s)=\frac{\theta_1 a_1 a\varepsilon}{(s+a_1)(s+a_3)}+\frac{(1-\theta_1)a_1}{(s+a_1)} \tag{18b}$$

$$\text{B1 to 3:}\quad G(s)=\frac{a_2}{(s+a_2)} \tag{18c}$$

where a_1, a_2, and a_3 are the respective reciprocals of the PSR mean residence times τ_1, τ_2, and τ_3, and θ_1 and θ_2 are the stream entrainment fractions shown in Figure 8. Several variations of the base model were also tried in an effort to improve the fit to the tracer data. All these models described the mixing section with five mixing parameters, in the same manner as Eqs. 18a–18c, and were consistent with the temperature and geometric observations. Each has minor variations from the base model, but maintains the same number of mixing parameters.

The model downstream of the choke describes the stream as it expands from a fast moving fluid in the narrow choke to the slower moving fluid downstream. Translating the model in Figure 8 downstream of the choke (that is, the burnout section) to a formula gives

$$\text{4 to 5:}\quad G(s)=\frac{a_4 e^{-\tau_5 s}}{(s+a_4)} \tag{19}$$

where a_4 is the reciprocal of τ_4. This assumes that the confluence of the kiln gas and burner streams is in the choke at point 4. However, the burnout section RTDs derived from tracers entering at the tangential entry points (points B1 and B2) into the mixing section had mean times 0.6 to 0.7 s shorter than the RTD produced from the axial entry point (point C). Figure 9 shows a model proposed to reconcile these differences. It considered the kiln gas and the burner gas streams as separate, which was consistent with the temperature profile in the choke. The model proposed that the burner gas stream, emerging from the center of the choke duct, forms a separate recirculating zone as the kiln gas bypasses this zone and mixes farther downstream.

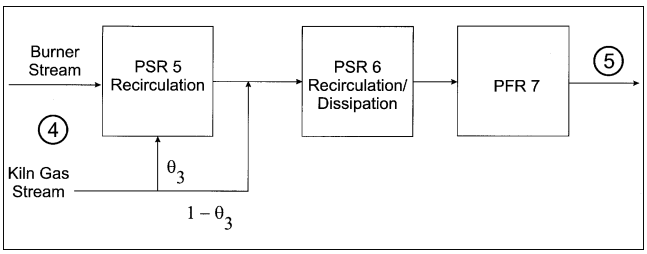

Figure 9. Alternate ideal reactor burnout section model (model 1b).

Error analysis

Estimation of the confidence bounds, allowing testing the sensitivity of the objective model to the errors of the mixing model parameters, can be useful for refinement or selection of the preferred candidate networks. Parameters with relatively high standard errors or high covariance often indicate overparameterization (Draper and Smith, 1998). The networked ideal reactor model estimates the normalized system response of the tracer $\hat{y}$. The ith estimated point $\hat{y}_i$ is a function of the independent variable x_i (which correspond to the discrete time measurements, $i\Delta t$, for $i = 0, 1, 2, 3, \ldots m-1$) and n parameters (α_1, α_2, α_3 ... α_n). The sensitivity of the parameters can be deduced from the covariance matrix, Ψ (Press et al., 1992). Diagonal elements of the covariance matrix give the standard or probable parameter variance, and their square roots give the standard or probable error of the parameters

$$\sigma(\alpha_j)=\sqrt{\Psi_{jj}} \tag{20}$$

The off-diagonal elements represent the covariance between parameters. Values near zero indicate a high degree of independence between parameters. An overparameterized model usually has some parameters with relatively high covariance between them (Draper and Smith, 1998). The standard errors do not give the confidence bounds. The confidence bounds can be calculated independently using the t-distribution, but these confidence intervals are misleading and inaccurate since they assume that parameters are independent of each other and have errors which are normally distributed, which is seldom the case for nonlinear least-squares estimation (Rooney and Biegler, 2001). Other methods that more accurately estimate the confidence region involve Monte Carlo techniques were not explored in this work.

Results and model selection — mixing section

Since parameters are shared in Eqs. 18a–18c, results were based on a simultaneous fit of all three equations. Table 3 shows the fitted parameters for two mixing section models: the base line model (model 0); and a variation that sets θ_2 equal to 1 and adds PFR 4 after PSR 3 (model 1a). The table lists the standard errors of the parameters and compares the derived model moments (mean, variance, and skewness) to the moments obtained from the reconstructed RTDs. The table also gives the standard deviation between the data and each fitted model for a standard of comparison. Both models show θ_1 as zero or near-zero, which implies a complete bypass between the flame zone and choke. The burner and kiln

Table 3. Results of Competing Mixing Section Models.

	Units	Model 0 (std error)	Model 1a (std error)	Reconstructed RTD
Standard deviation	s	0.040	0.028	
θ_1	none	0.005 (0.151)	0.000 (0.000)	
θ_2	none	1.000 (0.113)		
τ_1 (PSR)	s	0.330 (0.083)	0.333 (0.007)	
τ_2 (PSR)	s	0.561 (0.007)	0.560 (0.003)	
τ_3 (PSR)	s	0.596 (0.091)	0.003 (0.594)	
τ_4 (PFR)	s		0.552 (0.559)	
B1 to 4				
mean	s	1.16	1.12	1.08
variance	s^2	0.67	0.31	0.40
skewness	none	1.42	2.00	1.46
C to 4				
mean	s	0.33	0.33	0.31
variance	s^2	0.11	0.11	0.17
skewness	none	1.97	2.00	2.03
B1 to 3				
mean	s	0.56	0.56	0.57
variance	s^2	0.31	0.31	0.32
skewness	none	2.00	2.00	2.57

gases essentially do not mix inside the mixing section of the SCC. Additionally, none of the kiln gas bypasses PSR 3, which is implied by a value of unity for θ_2 in models 0. The fitted parameters of all models show a great deal of consistency with the moments derived from the reconstructed RTDs.

The first moments (mean) derived from the model parameters show excellent agreement (within the measurement interval of 0.05 s) with the mean calculated from the reconstructed RTDs. Higher-order moments, however, showed less agreement with some models. While the measurement of the variance from tracer data can be more problematic because it weights the data furthest from the mean, which is more affected by noise, lack of agreement is a criterion for eliminating other model variations.

Comparison of the skewness coefficients derived from the model parameters with those derived from the reconstructed RTDs reveals several trends. The single PSR has a skewness coefficient of 2.0. Both models have good agreement with the skewness coefficient from the reconstructed RTD for the flame (PSR 1) and tangential mixing area (PSR 2). The higher number from the reconstructed RTD for B1 to 3 could indicate long tails that result from dead space (Himmelblau and Bischoff, 1968) or simply an outlying data anomaly magnified by the higher moment. The skewness coefficient from the reconstructed RTD between B1 and 4 supports a model with two PSRs of approximately equal size as in model 0. However, the distinction is less clear when considering the standard error of the parameters.

Model 1a has high standard errors for τ_3 and τ_4. Because τ_3 and τ_4 are highly correlated, an alternate description of the model defined a new parameter τ_{34} as the mean residence time for the sum of PSR 3 and PFR 4, and τ_{34} as the fraction of that mean residence time in PSR 3. Defined in this manner, the parameter values become

$$\tau_{34} \quad 0.555 \quad (0.014)$$

$$\theta_{34} \quad 0.008 \quad (0.944)$$

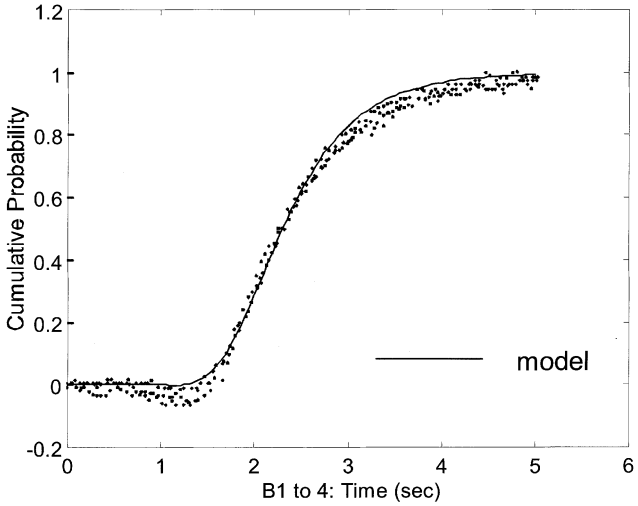

Figure 10. Comparison of Model 1a with normalized data: B1 to 4.

So, the residence time of the sum of PSR 3 and PSR 4 can be estimated with relatively high certainty, but it cannot be determined from the data where PSR 3 ends and PFR 4 begins with a reasonable degree of certainty. By considering it this way, if τ_3 is assigned a value of 0.350 and τ_4 is assigned a value of 0.205, then the B1 to 4 model variance becomes 0.44 and the skewness coefficient becomes 1.52, which is much closer to the respective reconstructed RTD values of 0.40 and 1.46. Thus, within the relative certainty of the parameters, model 1 provides the best fit and agreement with the RTD moments.

Figures 10 and 11 compare the model with the data, and the LS reconstructed RTD, respectively. Figure 10 shows evidence of a dead space effect of between 3 and 4 s where the model overshoots the data. The model was insufficiently complex (by design) to account for the slow absorption or desorption of tracer from a dead volume. By fitting on the 0

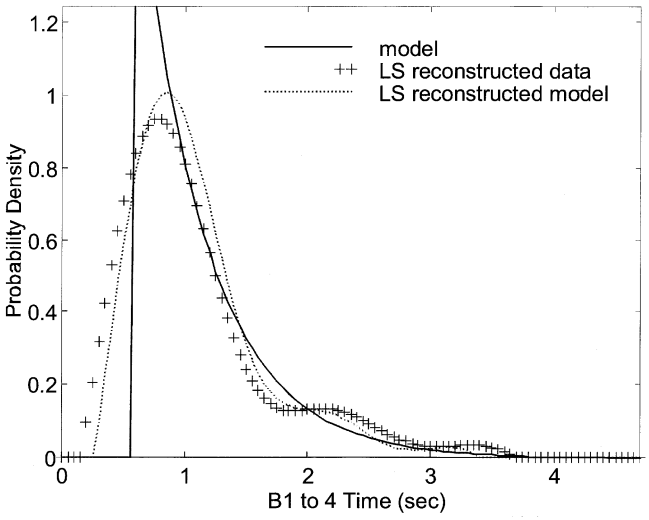

Figure 11. Comparison of Model 1a with LS reconstructed RTD: B1 to 4.

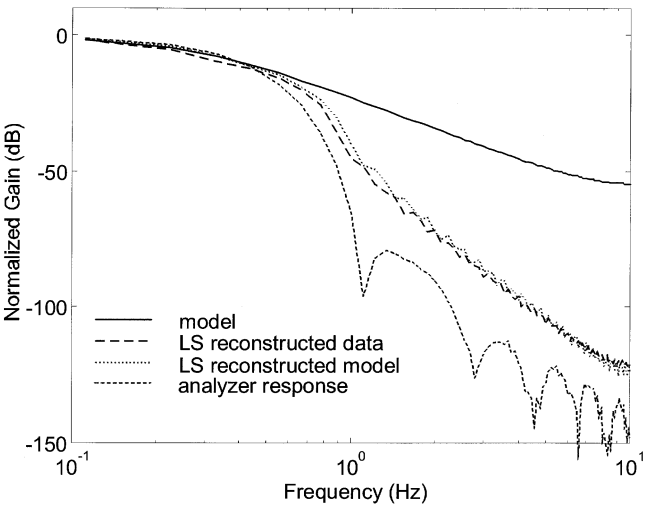

Figure 12. Power spectrum comparison of Model 1a and LS reconstructed RTD: B1 to 4.

to 2.7 s interval, the model parameters could be optimized for the portion they were meant to describe. Figure 11 shows the same comparison when the effect of the analyzer is removed from the system response. The effect of the LS reconstruction accounts for the large difference between model 1a and the reconstructed RTD. The dashed line shows the LS reconstructed result of the model 1a synthesized system response to illustrate this issue. Some information is lost in the reconstruction process from a band-limiting effect of the analyzer.

Figure 12 shows the power spectrum density of the analyzer compared to model 1a for the B1 to 4 input/output combination in the mixing section. The analyzer function has a gain reduction of 100 dB above 1 Hz. Since the analyzer function drives the response of the actual system, it dampens the frequencies above 1 Hz of the system response. As a result, the LS reconstructed data and the LS reconstructed model (the model driven by the analyzer response then reconstructed again) fail to match the power densities of the model at the higher frequencies. This effectively limits the LS reconstruction of both data and model to frequencies below 1 Hz.

This frequency band limitation produces nonunique solutions in the reconstruction process. For instance, the LS reconstructed data graphed in Figure 11 could have resulted from any one of a number of systems with power spectral densities equal to or below 1 Hz, but differing greatly above 1 Hz. The constrained iterative restoration algorithm (Schafer et al., 1981) applied for the RTD reconstruction took a consistent approach by starting with the system response (model or real system driven by the analyzer function) as the initial solution. By doing this, nothing is assumed in the solution about the higher frequencies.

Results and model selection — burnout section

For the burnout section, model 0 (Figure 8) assumed a completely mixed flow emerging from the choke, and model 1b (Figure 9) assumed a complete segregation of the kiln gas and burner gas streams. The parameters for model 0 could be fit using any tracer run measured downstream of the choke and a tracer run originating at the same input and measured at the choke as the driving function in the role of the analyzer function. Model 1b requires a simultaneous fit in the same manner as the mixing section. Model 0 was modified by replacing its single burnout section PSR with two equal PSRs in series (labeled PSR 5 for consistency). This provided the best fit and its results are presented in Table 4. Results produced from the B2/5 and C/5 tracer runs on model 0 are compared to the simultaneous parameter fitting on model 1b using the same tracer runs.

The results produced for model 0 from the different tracer inputs (B2 and C) varied by 0.77 s for total mean residence time. Even though each individually agrees with the reconstructed RTD, both cannot exist since different values are required for the same ideal reactors. Model 1b, which assumes segregated streams, resolves the contradiction by initially giving the streams two separate paths and allowing the mixing to occur farther downstream. The resulting first and second moments derived from the model parameters show good agreement with those corresponding to the reconstructed RTDs. Figure 13 shows the comparison between model 1b and the reconstructed RTD. As was the case with Figure 11, the reconstructed RTD and reconstructed model show good agreement, but the higher frequencies lost in the

Table 4. Results of Competing Burnout Section Models.

	Units	Model 0 (B2 input) (std error)	Model 0 (C input) (std error)	Model 1b (std error)	Reconst RTD
θ_3	none			0.013 (0.155)	
τ_5 (PSR)	s	0.782 (0.014)	0.898 (0.011)	0.765 (0.117)	
τ_6 (PSR)	s			1.102 (0.094)	
τ_7 (PFR)	s	0.811 (0.029)	1.345 (0.018)	1.287 (0.032)	
4 to 5 (B2 Input)					
Mean	s	2.37		2.40	2.27
variance	s^2	1.22		1.23	1.05
skewness	none	1.41		1.98	0.75
4 to 5 (C Input)					
Mean	s		3.14	3.15	2.99
variance	s^2		1.61	1.80	1.41
skewness	none		1.41	1.48	0.82

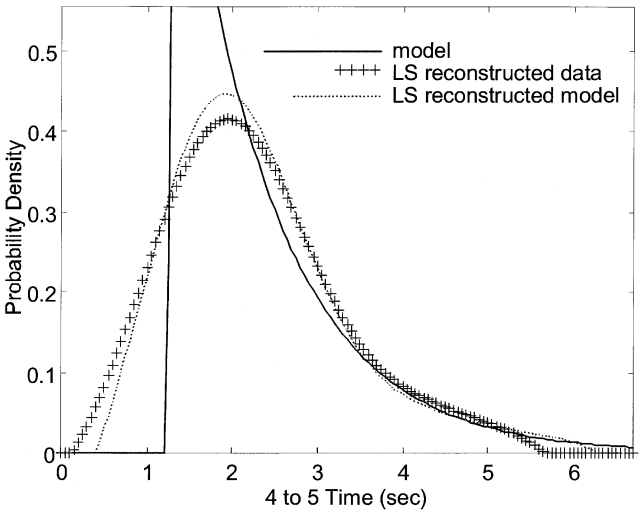

Figure 13. Comparison of Model 1b with LS reconstructed RTD: 4 to 5 w/ B2 input.

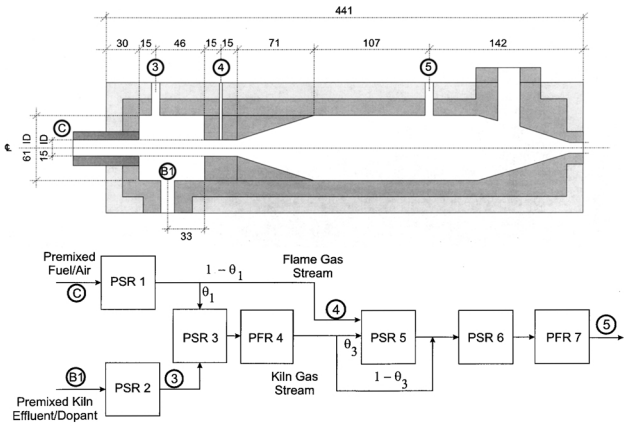

Figure 14. Selected model juxtaposed to physical secondary combustion chamber.

Dimensions in centimeters.

reconstruction process cause the difference with the impulse response of model 1b.

Temperature and volume parameters

Temperatures assigned using cross-section temperature profiles and energy balances enabled ideal reactor volumes to be determined. This enabled ideal reactor volumes to be determined, which is summarized in Table 5 for the chosen model (Figure 14). The difference between the active and physical volumes indicated the presence of 53 L of dead space in the 177 L mixing section, but found 37 L more active volume than the 410 L physical volume of the burnout section. However, overall there was good agreement between the identified model and the physical geometry of the SCC.

The evaluation of standard errors for the fitted parameters quantified the uncertainty in the model. Within the mixing section, standard errors were generally low (less than 0.01 s). The exceptions were the parameters for the two in-series reactors PSR 3 and PFR 4 on the kiln gas stream between points 3 and 4. Further analysis revealed that the standard error for the combined mean residence times was very small, but the uncertainty of the dimensionless fraction apportioning that time between the two reactors was very high (0.944 for a 0 to 1 scale). Since the PSR and PFR represent different extremes of ideal macromixing, this indicated a large degree of uncertainty in quantifying the mixing characteristics between points 3 and 4 in the kiln gas stream. Parameters in the burnout section had larger standard errors, but were less than 0.12 s for parameters ranging from 0.77 to 1.29 s. The standard error for the parameter describing the fraction of kiln gas stream mixing with the burner gas stream mixing in PSR 5 was the largest (0.155 for a 0 to 1 scale).

Table 5. Model Parameters: Residence Times, Temperatures, and Resulting Volumes.

Ideal Reactor	Mean Residence Time (s)	Temp. (K)	Vol. (L)
PSR 1	0.333	1,538	24.0
PSR 2	0.560	1,009	45.2
PSR 3	0.003	1,009	0.2
PFR 4	0.552	1,009 (in) 1,404 (out) 1,250 (LMT*)	55.1
PSR 5	0.765	1,451	53.1
PSR 6	1.102	1,323	184.8
PFR 7	1.287	1,323 (in) 1,241 (out) 1,281 (LMT)	209.0
Mixing Section			
(Physical System)	1.36	1,031	178
(Active System)	1.12		125
Burnout Section			
(Physical System)	3.13	1,342 (LMT)	410
(Active System)	2.39		447

*Log Mean Temperature

The residence time of the physical system was calculated in the same manner that would have been used for a design calculation of a commercial SCC. It was based on the total flow, averaged measured or log mean temperature, and physical volume. The active residence times considered only the path taken by the tracer-laden kiln gas. These calculations show that the active path, identified in the networked ideal reactor model, is 1 s shorter than the superficial residence time from the design calculations. Differences are also apparent between physical volumes from the SCC geometry and active volumes from the sum of ideal reactor volumes. The difference between the active and physical volume in the mixing section is likely manifested as dead space or dead volume. Early investigations of probe placements indicated the presence of dead space in the mixing section adjacent to the choke wall. The gradual expansion from the choke into the burnout section prevents dead space caused by the abrupt diameter change between the mixing section and choke. The derived active volume for the burnout section is actually greater than the physical volume. This is a likely result of experimental error in the tracer and temperature measurements and assumptions regarding the average temperatures of the ideal reactors in the chosen model. When placed in perspective, the error reflects a 0.28-s error in a 3.13-s burnout section.

Summary and Conclusions

A model was chosen based on the best fit to SO_2 tracer data and consistency with physical geometry, resulting flow patterns, and temperature measurements. A frequency bandwidth limitation introduced by the SO_2 analyzer precluded distinguishing solutions that differ only in the higher frequencies. Hence, a best-fit model does not represent a unique solution, and other considerations (such as reactor geometry, analysis of flow patterns and swirl, and temperature cross-section measurements) also merited equal consideration in model selection.

The tracer analysis revealed relatively poor mixing within the secondary combustion chamber. The analysis found that complete mixing between the kiln gas and burner stream occurs at some distance downstream of the choke. Since, a quasi-regulatory SCC design criterion is based on the average temperature and the superficial residence time, a compliant design might be insufficient to reburn rogue droplets or the transient puffs characterized by Lemieux et al. (1992). This underscores the importance of a choke or appropriate bluff body, which is not typically included, to enhance mixing within the SCC. It also suggests that different design criteria are in order to ensure complete combustion in practical secondary combustion chambers.

Acknowledgments

This work was supported by the Northeast Hazardous Substances Research Center at the New Jersey Institute of Technology (Newark, NJ), and the U.S. Environmental Protection Agency.

Literature Cited

Beér, J. M., and K. B. Lee, "The Effect of the Residence Time Distribution on the Performance and Efficiency of Combustors," *Tenth Symp. (Int.) on Combustion*, The Combustion Institute, Pittsburgh, PA, 1187 (1965).

Beér, J. M., and N. A. Chigier, *Combustion Aerodynamics*, Krieger Publishing, Malabar, FL (1983).

Draper, N. R., and H. Smith, *Applied Regression Analysis, 3rd Ed.*, Wiley, New York (1998).

Ewan, B. C. R., F. Boysan, and J. Swithenbank, "Closing the Gap Between Finite Difference and Stirred Reactor Combustor Modeling Procedures," *Twentieth Symp. (Int.) on Combustion*, Combustion Institute, Pittsburgh, PA, 541 (1984).

Fogler, S. H., *Elements of Chemical Reaction Engineering, 2d Ed.*, Prentice-Hall, Englewood Cliffs, NJ (1992).

Fristrom, R. M., *Flame Structure and Processes*, Oxford University Press, New York (1995).

Hallett, W. L. H., "Swirl Generator for Independent Variation of Swirl and Velocity Profile," *AIAA J.*, **24**, 1212 (1986).

Himmelblau, D. M., and K. B. Bischoff, *Process Analysis and Simulation, Deterministic Systems*, Wiley, New York (1968).

Hsia, T. C., *System Identification: Least-Squares Methods*, Lexington Books, Lexington, MA (1977).

Lemieux, P. M., W. A. Linak, J. A. McSorley, and J. O. L. Wendt, "Transient Suppression Packaging for Reduced Emissions from Rotary Kiln Incinerators," *Combustion Science and Technology*, **85**, 203 (1992).

Lemieux, P., J. Ryan, C. Bass, and R. Barat, "Emissions of Trace Products of Incomplete Combustion from a Pilot-Scale Incinerator Secondary Combustion Chamber," *J. of the Air and Waste Management Association*, **46**, 309 (1996).

Levenspiel, Octave, *Chemical Reaction Engineering, 2d Ed.*, Wiley, New York (1972).

Nasserzadeh, V., J. Swithenbank, C. Schofield, D. W. Scott, and A. Loader, "Effects of High Speed Jets and Internal Baffles on the Gas Residence Times in Large Municipal Incinerator," *Environmental Prog.*, **13**, 124 (1994).

Nelder, J. A., and R. Mead, "A Simplex Method for Function Minimization," *Computer J.*, **7**, 308 (1965).

Press, W. H., S. A. Teukolsky, W. T. Vetterling, and B. P. Flannery, *Numerical Recipes in C, the Art of Scientific Computing, 2d Ed.*, Cambridge University Press, Cambridge, U.K. (1992).

Ravichandran, M., and F. C. Gouldin, "Residence Time Calculations Using Numerical Simulation of Incineration Flows," *Combustion Science and Technol.*, **91**, 257 (1993).

Rooney, W. C., and L. T. Biegler, "Design for Model Parameter Uncertainty Using Nonlinear Confidence Regions," *AIChE J.*, **47**, 1794 (2001).

Schafer, R. W., R. M. Mersereau, and M. A. Richards, "Constrained Iterative Restoration Algorithms," *Proc. of IEEE*, **69**, 432 (1981).

Swithenbank, J., I. Poll, M. W. Vincent, and D. D. Wright, "Combustion Design Fundamentals," *Fourteenth Symp. (Int.) on Combustion*, Combustion Institute, Pittsburgh, PA, 627 (1972).

Syred, N., and J. M. Beér, "Combustion in Swirling Flows: A Review," *Combust. and Flame*, **23**, 143 (1974).

Manuscript received Sept. 30, 2002, and revision received Mar. 25, 2003.